Hybrid Fiber-Optic Radio Frequency and Optical Frequency Dissemination With a Single Optical Actuator and Dual-Optical Phase Stabilization

Xueyang Tian, Liang Hu, *Member, IEEE*, Guiling Wu, *Member, IEEE*, and Jianping Chen

***Abstract*—In this paper, we propose and experimentally demonstrate a technique for simultaneous dissemination of optical and radio frequencies (RF) over an optical-fiber link with a single optical actuator and dual-optical phase stabilization. The optical actuator, namely electro-optic modulator (EOM), can simultaneously be served with a coupler and a dual optical frequency shifter to couple an RF frequency and an optical frequency and to efficiently suppress the phase noise of the two optical frequencies introduced by the fiber link with dual-optical phase stabilization, respectively. We experimentally demonstrate 193 THz optical carrier dissemination with a stability of 1.2×10^{-15} at the integration time of 1 s and 3.5×10^{-17} at 10,000 s, and 0.9 GHz RF frequency dissemination with a stability of 5.7×10^{-13} at 1 s and 5.2×10^{-16} at 10,000 s over a 30 km optical fiber link in a single telecommunication channel. This proof-of-principle experiment is particularly useful for users who need both RF and optical frequencies simultaneously, but do not have cumbersome and expensive optical combs, and also provides a promising solution towards a robust and flexible ultrastable optical frequency network for multi-user dissemination based on a frequency division multiplexing technique.**

***Index Terms*—Metrology, optical fiber, optical frequency transfer, radio frequency transfer.**

I. Introduction

FIBER-OPTIC time and frequency dissemination has attracted widespread research interest. Thanks to the rapid development over the last decades, newly developed radio frequency (RF) and optical frequency dissemination schemes with ever-increasing performance and fiber distances are expected to play a crucial role for science and technology including geodesy [1], radio astronomy [2], [3], optical clock comparisons [4], [5] and tests of fundamental physics [6], [7]. Up to now, a bunch of methods has been investigated for dissemination of RF frequencies and optical frequencies over optical fiber networks. An RF frequency can be transferred to the remote user sites by amplitude modulating a continuous-wave (CW) laser before it is sent through a fiber link [8]–[10]. An optical carrier wave itself can also be disseminated by transferring the light of a stable CW laser [11]–[17]. Furthermore, RF and optical frequencies can be disseminated simultaneously by transmitting pulses from a mode-locked laser [18]–[21]. Among them, optical carrier-based frequency dissemination has the best performance because of its high carrier frequency and no fiber dispersion effect [11]–[17].

While fiber-optic optical frequency dissemination provides a superior fractional frequency stability over fiber-optic RF transmission [12]–[15], the existing commercial atomic clocks and frequency standards are still dominated by microwave atomic clocks, and many applications in science, commerce, and industry require an RF frequency in order to provide a stable RF source for their electronic systems or electro-optical components like acousto-optic modulators (AOMs) [7]. The conversion from the optical frequency to the RF frequency can be achieved by adopting optical frequency combs. The combs, however, are usually expensive and cumbersome [22], [23], limiting their promotion and applications, especially, in space. Therefore, the range of applications and experiments supported by optical frequency transfer networks can be improved by the direct provision of a stabilized RF frequency. In addition, towards the definition of SI second based on optical atomic transitions by verifying optical atomic clocks being compatible with the current definition, namely the microwave hyperfine transition in ^{133}Cs, it is necessary to compare the absolute frequency between candidate optical standards and primary cesium references. To perform this task, high-precision RF frequency and optical frequency comparison techniques are simultaneously necessary [24]–[27].

Various techniques for transferring RF and optical frequencies simultaneously based on optical fiber as a transmission medium have been rapidly developed. In principle, the RF and optical frequencies can be disseminated by using two independent systems with a wavelength division multiplexing (WDM) technique, but this will sacrifice the valuable fiber capacity resource and increase the complexity of the apparatus. Feng *et al.* demonstrated a technique for simultaneous transferring of optical and RF frequencies over a fiber link by simply cascading the RF phase stabilization and optical phase stabilization systems [28].

Manuscript received November 18, 2019; revised February 11, 2020 and March 31, 2020; accepted April 18, 2020. Date of publication April 21, 2020; date of current version July 28, 2020. This work was supported in part by the National Natural Science Foundation of China under Grants 61627871, 61535006, 61905143, and in part by Science and Technology project of State Grid Corporation of China (No. SGSHJX00KXJS1901531). *(Corresponding authors: Liang Hu; Guiling Wu.)*

Xueyang Tian, Liang Hu, Guiling Wu, and Jianping Chen are with the State Key Laboratory of Advanced Optical Communication Systems and Networks, Department of Electronic Engineering, Shanghai Jiao Tong University, Shanghai 200240, China, and also with the Shanghai Institute for Advanced Communication and Data Science, Shanghai Jiao Tong University, Shanghai 200240, China, and also with the Shanghai Key Laboratory of Navigation and Location-Based Services, Shanghai 200240, China (e-mail: txy0220@sjtu.edu.cn; liang.hu@sjtu.edu.cn; wuguiling@sjtu.edu.cn; jpchen62@sjtu.edu.cn).

Color versions of one or more of the figures in this article are available online at https://ieeexplore.ieee.org.

Digital Object Identifier 10.1109/JLT.2020.2989328

0733-8724 © 2020 IEEE. Personal use is permitted, but republication/redistribution requires IEEE permission.
See https://www.ieee.org/publications/rights/index.html for more information.

Authorized licensed use limited to: Shanghai Jiaotong University. Downloaded on February 06,2021 at 13:16:32 UTC from IEEE Xplore. Restrictions apply.

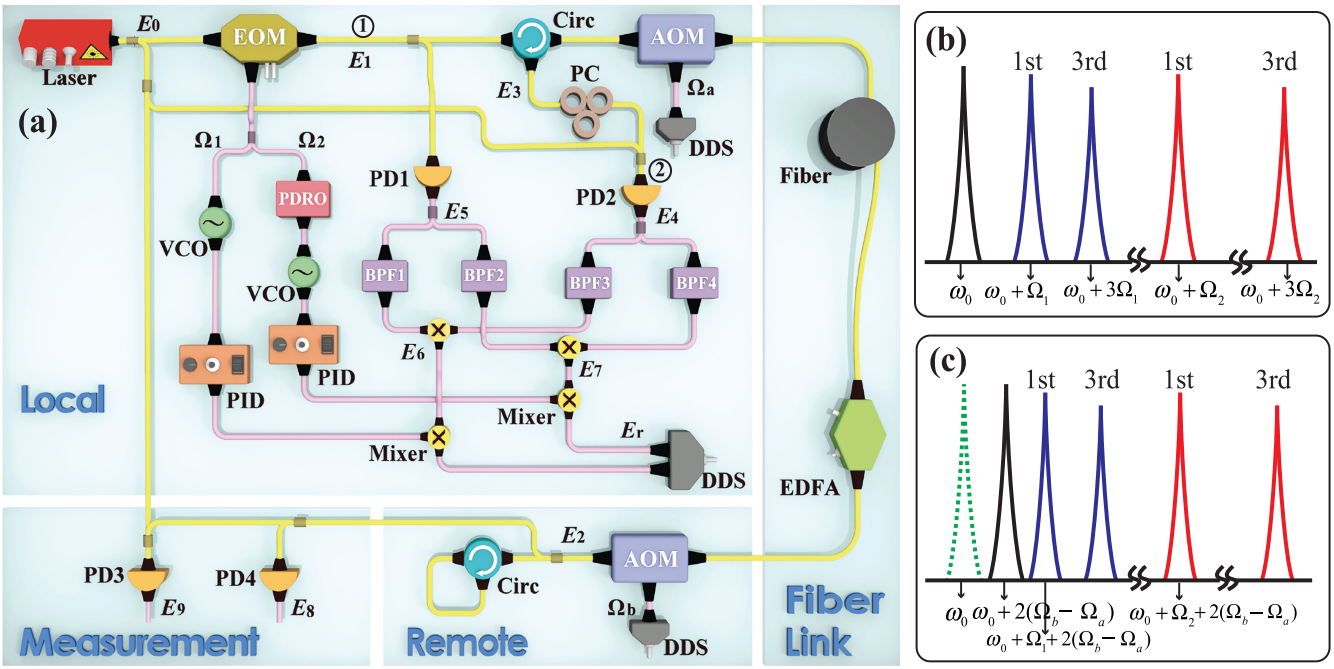

Fig. 1. (a) Schematic diagram of our hybrid fiber-optic RF frequency and optical frequency dissemination with a single optical actuator and dual-optical phase stabilization. (b) Optical spectrum diagram just after the EOM biased as $V_\pi/2$ as the "①" indicated in (a). (c) Optical spectrum diagram just before PD2 as the "②" indicated in (a). EOM: electro-optic modulator, AOM: acousto-optic modulator, EDFA: erbium-doped fiber amplifier, DDS: direct-digital synthesizer, Circ: optical circulator, PD: photodetector, PDRO: phase-locked dielectric resonator oscillator, VCO: voltage-controlled oscillator, BPF: band-pass filter, PID: proportional-integral-derivative controller, PC: polarization controller.

Krehlik *et al.* proposed and demonstrated a hybrid solution for simultaneous dissemination of an optical frequency, an RF frequency, and a time signal over an optical fiber in which they combined the standard phase-stabilized optical carrier transfer with the electronically stabilized (ELSTAB) technology designed for delay-stabilized transfer of the RF frequency reference and the one pulse per second (1 PPS) time signal [29]. Both above solutions adopted two different wavelengths on two directions for avoiding the effect of the Rayleigh backscattering on the RF transfer stability. Schediwy *et al.* proposed a method of simultaneous transferring of optical and RF frequencies over the optical fiber link [30], in which two AOMs as two frequency actuators are used for independently correcting the phase noise of two optical carrier signals. The two optical frequencies are separated by an RF frequency achieved by using an additional dual-parallel Mach-Zehnder modulator (DPMZM). Although it only occupies one telecommunication channel, the use of the two independent AOMs and the additional DPMZM will induce uncommon-mode phase noise on the stabilized RF frequency since two optical signals experience different optical paths at the local site [30]. Additionally, the limited carrier and sideband suppression ratio produced by the DPMZM will introduce the crosstalk phase noise on the stabilized RF frequency [31].

The paper is organized as follows: section II describes the proposed hybrid fiber-optic RF and optical frequencies dissemination technique; in section III the experimental apparatus and the main experimental results are presented, including an assessment of RF frequency transfer performance and optical frequency dissemination performance; section IV discusses main limitation of the present apparatus and the feasible solutions for future improvements; finally, in section V a conclusion is given.

II. Concept of the Hybrid System

The underlying idea of the solution proposed here is to simultaneously transfer RF and optical frequencies by using a single optical actuator, namely a Mach-Zehnder-type electro-optic modulator (EOM) and two standard optical phase stabilization setups as shown in Fig. 1(a). To satisfy this, the EOM is driven by two RF signals at angular frequencies of Ω_1 and Ω_2, resulting in its output where the dual 1st sidebands differ by $\Omega_0 = \Omega_2 - \Omega_1$ as illustrated in Fig. 1(b). This way, two conventional optical stabilization servo systems are used to independently correct two optical signals by tuning the frequency of the two RF signals. This creates two, independently stabilized optical signals that are separated by a given RF frequency of Ω_0. In this approach, both optical frequencies follow the same optical path; thus, the same phase fluctuations that may be caused, for example, by vibrations, temperature fluctuations, etc. on the fiber path at the local site, will be superimposed onto the two optical frequencies, and do not degrade the phase noise in the difference frequency of Ω_0. Moreover, the technique presented here uses a single optical actuator, so it is able to benefit from the advantages of optical frequency dissemination in terms of the reduced size and complexity of the stabilization equipment.

Figure 1 illustrates a schematic view of the proposed fiber-optic RF and optical frequencies dissemination technique. The optical signal $E_0 \propto \cos(\omega_0 t)$ from a laser is fed into an EOM

Authorized licensed use limited to: Shanghai Jiaotong University. Downloaded on February 06,2021 at 13:16:32 UTC from IEEE Xplore. Restrictions apply.

biased at $V_\pi/2$. Here and in the following text, the amplitude and the initial phase are ignored for clarity. The modulated optical signal is determined by two RF signals with angular frequencies of Ω_1 and Ω_2 and corresponding correctional phase shifts ϕ_{c1} and ϕ_{c2} for the dual 1st sidebands with angular frequencies of $\omega_0+\Omega_1$ and $\omega_0+\Omega_2$, respectively, as the optical spectrum diagram illustrated in Fig. 1(b). The correctional phase shifts are decided by the feedback from the servo electronics. The modulated output can be expressed as,

$$E_1 \propto \exp[j\omega_0 t] \times \cos\left[\frac{\pi}{4} + m_1\cos(\Omega_1 t+\phi_{c1}) + m_2\cos(\Omega_2 t+\phi_{c2})\right],$$

where m_1 and m_2 are the modulation indexes for the two RF frequencies, respectively.

The modulated optical signal after passing through a local AOM (downshifted mode, -1 order) is launched into an optical fiber link. Once it passes through the fiber link, the different optical frequencies will accumulate different phase fluctuations coming from environmental perturbations on the fiber link. At the remote site, the light encounters a remote AOM (upshifted mode, $+1$ order) used to separate the desired round-trip signal from spurious reflections on the fiber link, and then the signal becomes,

$$E_2 \propto \exp[j((\omega_0-\Omega_a)(t-\tau_0)+\Omega_b t)] \times \cos\left[\frac{\pi}{4} + m_1\cos(\Omega_1(t-\tau_0)+\phi_{c1}) + m_2\cos(\Omega_2(t-\tau_0)+\phi_{c2})\right],$$

where τ_0 is the propagation delay introduced by the fiber link L, and Ω_a and Ω_b are the working frequencies of the AOMs fed by a direct-digital synthesizer (DDS).

At the remote site, the signal is split into two paths, with one set of the signal going to photodetectors (PD3 and PD4) and the other is reflected from the remote site by an optical circulator, and returns along the same fiber link to the transmitter. We assume that the backward signal experiences the same phase fluctuations as the forward signal along the fiber link. The returned optical signal arrived at the PD2 can be written as,

$$E_3 \propto \exp[j(\omega_0(t-2\tau_0)+2(\Omega_b-\Omega_a)(t-\tau_0))]\cos\left[\frac{\pi}{4} + m_1\cos(\Omega_1(t-2\tau_0)+\phi_{c1}) + m_2\cos(\Omega_2(t-2\tau_0)+\phi_{c2})\right].$$

At the low modulation index condition, namely $m_1, m_2 \ll 1$, the signal after mixing E_3 and E_0 as the solid curves and the dotted curve shown in Fig. 1(c) onto the PD2 at the local site is expressed in E_4. Here the first term in E_4 represents the mutual-beat signals between the returned sidebands in E_3 and E_0, the second and third terms in E_4 come from the self-beat signals of E_3 and the last term is the mutual-beat signals between the returned carrier in E_3 and E_0. As the optical spectrum diagram illustrated in Fig. 1(c), we are only interested in two RF signals with angular frequencies of $\Omega_1+2(\Omega_b-\Omega_a)$ and $\Omega_2+2(\Omega_b-\Omega_a)$ in the first term in E_4. Both frequencies can be effectively filtered out by using band-pass filters.

Due to the unidirectional transmission characteristic of the EOM, the error signal can not be directly acquired by comparing the E_4 with standard RF signals. Here we introduce assistant signals by beating E_1 at the PD1, resulting in,

$$E_5 \propto \sum_{i=1}^{2}\sum_{m=1}^{\infty}\cos[(2m-1)(\Omega_i t+\phi_{ci})] + \sum_{m=1}^{\infty}\sum_{n=1}^{\infty}\cos[|(2n-1)\Omega_2-(2m-1)\Omega_1|t+|(2n-1)\phi_{c2}-(2m-1)\phi_{c1}|].$$

Afterwards, electronic band-pass filters (BPFs) after the PDs (PD1 and PD2) are used to reject the unwanted components from the desirable terms in E_4 and E_5. The two RF signals with angular frequencies of Ω_1 (BPF1) and $\Omega_1+2(\Omega_b-\Omega_a)$ (BPF3) are directly mixed and the upper sideband signal E_6 with an angular frequency of $2(\Omega_1-\Omega_a+\Omega_b)$ is filtered out by another bandpass filter. Other two RF signals with angular frequencies of Ω_2 (BPF2) and $\Omega_2+2(\Omega_b-\Omega_a)$ (BPF4) are also mixed and the upper sideband signal is extracted by cascading an additional BPF to produce a desirable signal E_7 with an angular frequency of $2(\Omega_2-\Omega_a+\Omega_b)$. E_6 and E_7 have expressions of,

$$E_6 \propto \cos[2(\Omega_1-\Omega_a+\Omega_b)(t-\tau_0)+2\phi_{c1}-2\omega_0\tau_0],$$
$$E_7 \propto \cos[2(\Omega_2-\Omega_a+\Omega_b)(t-\tau_0)+2\phi_{c2}-2\omega_0\tau_0].$$

In the next, E_6 and E_7 are, respectively, mixed with two standard RF signals with angular frequencies of $2(\Omega_1-\Omega_a+\Omega_b)$ and $2(\Omega_2-\Omega_a+\Omega_b)$ to produce error signals. Both standard RF frequencies are generated by the same DDS generator. Each DC part of the mixed signals is low-pass filtered to reject higher-frequency mixing products and then fed into a voltage-controlled oscillator (VCO) by using a proportional-integral-derivative (PID) controller. One VCO output, which is equal to Ω_1, is directly used to drive the EOM and the other one before driving the EOM is multiplied to Ω_2 by adopting a phase-locked dielectric resonator oscillator (PDRO). As a result, the magnitude of ϕ_{ci} are such that they cancel the phase noise for two optical frequencies

$$E_4 \propto \sum_{i=1}^{2}\sum_{m=1}^{\infty}\cos[((2m-1)\Omega_i+2(\Omega_b-\Omega_a))t+(2m-1)\phi_{ci}-2(\omega_0+(2m-1)\Omega_i-\Omega_a+\Omega_b)\tau_0] + \sum_{i=1}^{2}\sum_{m=1}^{\infty}\cos[(2m-1)\Omega_i(t-2\tau_0)+(2m-1)\phi_{ci}] + \sum_{m=1}^{\infty}\sum_{n=1}^{\infty}\cos[|(2n-1)\Omega_2-(2m-1)\Omega_1|(t-2\tau_0)+|(2n-1)\phi_{c2}-(2m-1)\phi_{c1}|] + \cos[2(\Omega_b-\Omega_a)t-2(\omega_0-\Omega_a+\Omega_b)\tau_0]$$

Authorized licensed use limited to: Shanghai Jiaotong University. Downloaded on February 06,2021 at 13:16:32 UTC from IEEE Xplore. Restrictions apply.

resulting from a single pass of the fiber link,

$$\phi_{c1} = (\omega_0 + \Omega_1 - \Omega_a + \Omega_b)\tau_0,$$
$$\phi_{c2} = (\omega_0 + \Omega_2 - \Omega_a + \Omega_b)\tau_0.$$

By substituting these equations into E_2, the result can be expressed as,

$$E_2' \propto \sum_{i=1}^{2}\sum_{m=1}^{\infty} \cos[(\omega_0 + (2m-1)\Omega_i - \Omega_a + \Omega_b)t + 2(m-1)(\omega_0 - \Omega_a)\tau_0 + (2m-1)\Omega_b\tau_0] + \cos[(\omega_0 - \Omega_a + \Omega_b)t - (\omega_0 - \Omega_a)\tau_0].$$

Here the second term represents the carrier of the modulated signal arriving at the remote site. Therefore at the remote site, the phase noise resulting from phase perturbations on the fiber link is largely suppressed for both of the optical frequencies with angular frequencies of $\omega_0 + \Omega_1 - \Omega_a + \Omega_b$ and $\omega_0 + \Omega_2 - \Omega_a + \Omega_b$ at the condition of $m = 1$, respectively. Note that some contamination is coming from the remaining phase noise term of $\Omega_b\tau_0$, which is about six orders of magnitude smaller than that of $\omega_0\tau_0$ and can be neglected for both optical frequencies. Each stabilized optical frequency can be filtered out by using optical phase-locked loop (OPLL) techniques [32].

At the same time, we can recover a stabilized RF frequency by self-beat E_2' at the PD4, resulting in,

$$E_8 \propto \sum_{m=1}^{\infty}\sum_{n=1}^{\infty} \cos[|(2n-1)\Omega_2 - (2m-1)\Omega_1|t + 2|n-m|(\omega_0 - \Omega_a + \Omega_b)\tau_0] + \sum_{i=1}^{2}\sum_{m=1}^{\infty} \cos[(2m-1)\Omega_i t + (2m-1)(\omega_0 - \Omega_a + \Omega_b)\tau_0].$$

Here the second term represents the beat frequency components between the modulated sidebands and the carrier in E_2'. Note that at the remote site, the phase noise resulting from phase perturbations on the fiber link is suppressed for the RF signal with an angular frequency of $\Omega_0 = \Omega_2 - \Omega_1$ when $n = m = 1$ in E_8.

To effectively evaluate the performance of optical frequency dissemination, we mix the optical signal E_2' at the remote site with the local signal E_0 onto the PD3. The beating results have an expression of,

$$E_9 \propto \sum_{i=1}^{2}\sum_{m=1}^{\infty} \cos[((2m-1)\Omega_i - \Omega_a + \Omega_b)t + 2(m-1)(\omega_0 - \Omega_a)\tau_0 + (2m-1)\Omega_b\tau_0] + \cos[(\Omega_b - \Omega_a)t - (\omega_0 - \Omega_a)\tau_0] + E_8.$$

Here the second term represents the mutual-beat signals between the transferred carrier signals in E_2' and E_0. With the assistance of bandpass filters, we can effectively filter out two RF signals with angular frequencies of $\Omega_1 - \Omega_a + \Omega_b$ and $\Omega_2 - \Omega_a + \Omega_b$ in E_9 to evaluate both transferred optical frequencies.

Note that the harmonics of the lower RF signal Ω_1 in E_4, E_5 and E_9 could be superimposed on the higher RF signal Ω_2 in E_4, E_5 and E_9 when the drifts of the EOM bias voltage from the ideal position at $V_\pi/2$ and the two RF signals have a multiple relationship, e.g., $\Omega_2 = k\Omega_1$ (k is an integer). This effect can be largely suppressed by using the two RF signals with a high ratio relationship because the amplitude significantly decreases with the increase of the harmonic order or by adopting the two RF signals without the multiple relationship.

III. Experimental Apparatus and Results

A. Experimental Apparatus

To verify the principle of the proposed scheme, a 30 km optical fiber spool in the laboratory frequency dissemination system is demonstrated. The whole system is placed in the laboratory with a temperature fluctuation of 3 °C, which is mainly due to our poor air conditioning system and human activities during the day. The local and remote sites are co-located, allowing an independent measurement of the frequency transfer stability of the three frequencies (two stabilized optical frequencies and one stabilized RF frequency). An optical carrier (NKT, X15) at 1550 nm ($\omega_0 \simeq 2\pi \times 193$ THz) with a linewidth of ~ 100 Hz is injected into an EOM made of LiNbO3 with a typical electrical bandwidth of 10 GHz and an insertion loss of 8 dB. To avoid nonlinear effects, the signal power launched into the fiber link is kept low (0 dBm in our case). Considering the experimental devices in our laboratory, we chose two RF signals as $\Omega_1 = 100$ MHz and $\Omega_2 = 1$ GHz. As the high frequency difference between Ω_1 and Ω_2, leading to that the phase noise of the 10th harmonic of Ω_1 on the Ω_2 can be ignored. Then they are combined by a power combiner and sent to the RF port of the EOM, where their modulation depths m_1 and m_2 are both close to 20%. The EOM is biased at $V_\pi/2$, resulting in a 0.9 GHz frequency difference between two optical sidebands in the 1st order as illustrated in Fig. 1(b). The local site AOM (downshifted mode, -1 order) and the remote site AOM (upshifted mode, +1 order) are working at the angular frequencies of $\Omega_a = 2\pi \times 40$ MHz and $\Omega_b = 2\pi \times 80$ MHz, respectively. Thus, the central frequencies of the 4 BPFs after the PD1 and the PD2 with the 3 dB bandwidth of 10 MHz are 100 MHz, 1 GHz, 180 MHz, 1.08 GHz, respectively. Additionally, two RF signals with the angular frequencies of $\Omega_1 - \Omega_a + \Omega_b = 140$ MHz and $\Omega_2 - \Omega_a + \Omega_b = 1.04$ GHz are used to evaluate the performance of optical frequency transfer. All the reference signals are synchronized to a Rb clock with a stability of 1.5×10^{-11} at 1 s. This configuration could guarantee the achieved optical frequency transfer stability of $\sim 10^{-17}$ at 1 s. The long term stability is mainly limited by the frequency asymmetry between the bidirectional optical signals and the stability of the uncompensated optical signal as discussed in [33].

At the remote site, a custom-made bidirectional erbium-doped fiber amplifier (EDFA) is used to compensate the forward optical signal due to the insertion loss of the EOM and other optical devices and to amplify the returned optical signal. For Doppler phase noise cancellation, we used PID controllers with second-order loop filters.

Authorized licensed use limited to: Shanghai Jiaotong University. Downloaded on February 06,2021 at 13:16:32 UTC from IEEE Xplore. Restrictions apply.

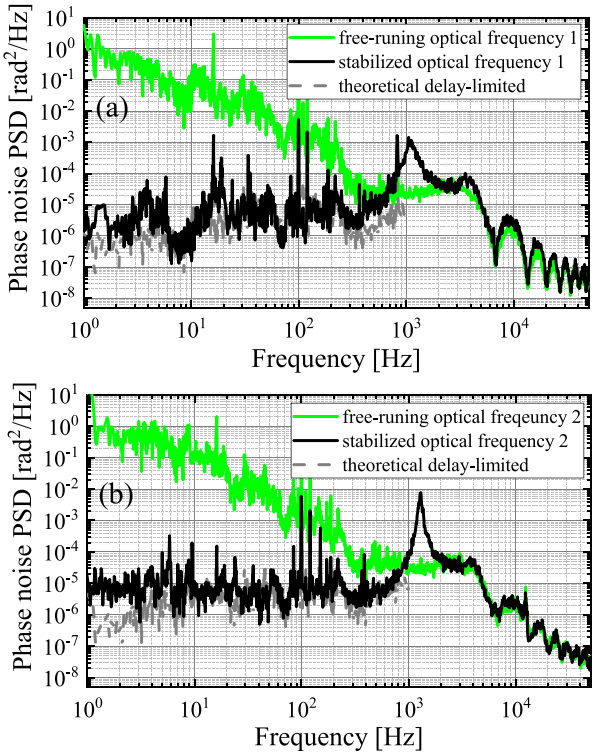

Fig. 2. Measured phase noise PSDs of the 30 km free-running optical frequency (green curves), $S_{\text{fiber}}(f)$, and stabilized optical frequency with fiber noise cancellation (black curves), $S_{\text{remote}}(f)$, for the optical frequency 1 (a) and the optical frequency 2 (b). The gray dashed curves are the theoretical prediction by using Eq. (1).

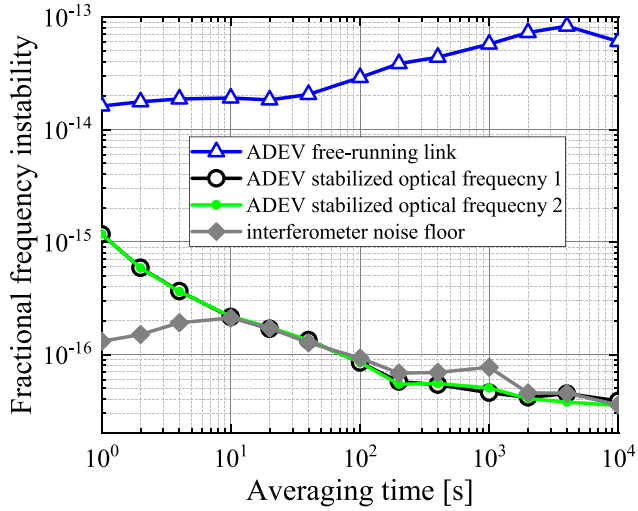

Fig. 3. Measured fractional frequency stability of optical frequency dissemination as a function of time. The blue curve with open triangle markers illustrates the instability of free-running optical frequency whereas the curves with open and filled circles indicate the fraction frequency stability of the signals with the fiber noise cancellation for the first (empty black circle markers) and second (filled green circle markers) optical frequencies, respectively. The curve with filled diamonds illustrates the interferometer noise floor.

We measured the stability of the remote two optical frequencies with a K+K FXE phase recorder and the stabilized RF frequency with a Microsemi 5120 A. Both devices are referenced to a standard RF frequency produced by the local DDS generator. Here to ensure its long-term transfer performance, we need to manually adjust the polarization approximately every half-day. However, unlike the K+K FXE used to evaluate optical frequency transfer, which can count without intervals, significant power and frequency fluctuations due to polarization adjustment will cause the Microsemi 5120 A to suspend the measurement. In the next step, an automatic polarization tracker is planned to be installed to reduce the polarization effects and measure the RF stability longer than 10^4 s. To measure the phase noise of the two optical frequencies, we perform the measurement by feeding the heterodyne beat detected by the PD3 illustrated in Fig. 1 together with a stable RF frequency reference to a phase detector. The voltage fluctuations at the phase detector output are then measured with a fast Fourier transform (FFT) analyzer to obtain the phase fluctuations $S_\phi(f)$. We determine the phase noise PSD, $S_{\text{remote}}(f)$, for the stabilized frequency and, $S_{\text{fiber}}(f)$, for the free-running frequency where no noise cancellation was applied.

B. *Optical Frequency Transfer*

Figure 2 shows a widespread frequency-domain characterization of phase instability, which is the power spectral density (PSD) of phase fluctuations $S_\phi(f) = |\tilde{\phi}(2\pi f)|^2$ with the Fourier transform normalized to the measurement time of the phase $\phi(t)$ between the sent and transferred optical waves. The phase noise PSDs of both optical frequencies have been measured for the stabilized optical frequency (black curve), and for the free-running optical frequency (green curve), where no phase noise cancellation was applied. We find that unlocked phase noise on our fiber link approximately follows a power-law dependence, $S_{\text{fiber}}(f) \sim h_0/f^2$ ($h_0 \simeq 3$), for $f < 1$ kHz, indicating that white frequency noise is dominating in the free-running optical frequency. By activating the fiber noise cancellation setup, the phase noise PSD, $S_{\text{remote}}(f)$, approaches another power-law dependence of h_{-2}/f^0 ($h_{-2} \simeq 6 \times 10^{-6}$), showing the remaining noise is mainly determined by the white phase noise. From Fig. 2, we also can find the measured locked phase noise to be in good agreement with the theoretical value (gray curves) predicted by [13],

$$S_{\text{remote}}(f) \approx \frac{1}{3}(2\pi f \tau_0)^2 S_{\text{fiber}}(f). \tag{1}$$

We can clearly see that the phase noise cancellation system suppresses the noise within its delay-unsuppressed below $\sim$ 1 kHz and strong servo bumps appear. The shifted bump position from the theoretical one ($1/(4\tau_0) \simeq 1.7$ kHz) is mainly coming from an additional delay from each unoptimized PID controller and RF components.

Complementary to the frequency-domain feature, a time-domain characterization of the frequency stability (Allan deviation) is shown in Fig. 3. In this plot, blue curve with open triangle markers indicate the fractional frequency instability of optical frequency dissemination at the remote site when the servo is not engaged. Curves with circle markers represent the stability of the optical frequencies with active stabilization. With the

Authorized licensed use limited to: Shanghai Jiaotong University. Downloaded on February 06,2021 at 13:16:32 UTC from IEEE Xplore. Restrictions apply.

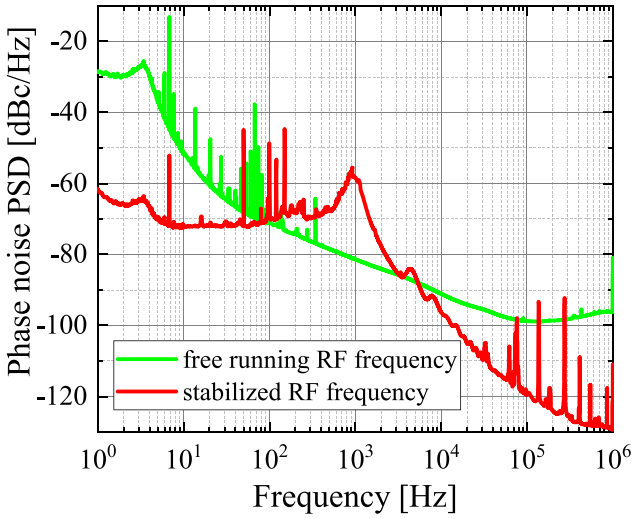

Fig. 4. Measured phase noise PSD of the 30 km free-running RF frequency (green curve) and stabilized RF frequency with fiber noise cancellation (red curve).

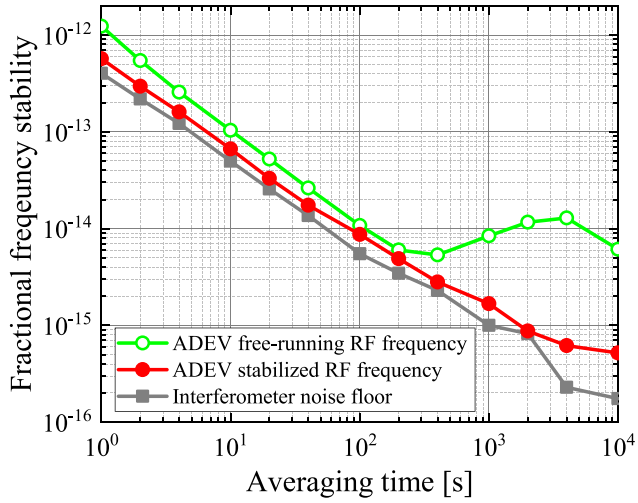

Fig. 5. Measured fractional frequency stability of RF frequency dissemination versus time. The green curve with open circle markers illustrates the instability of the 30 km free-running RF frequency whereas the curves with filled circles and squares represent the fractional frequency stability of the signals with fiber noise cancellation and the noise floor of the interferometer, respectively.

implementation of the fiber noise cancellation setup over a 30 km fiber link, the optical frequency 1 with the angular frequency of $\omega_0 + \Omega_1 - \Omega_a + \Omega_b$ achieves a fraction frequency instability of 1.2×10^{-15} at the integration time of 1 s and 3.5×10^{-17} at 10,000 s, whilst the second stabilized optical frequency with the angular frequency of $\omega_0 + \Omega_2 - \Omega_a + \Omega_b$ has the similar performance. We can clearly see that when the fiber noise cancellation setups are engaged, the frequency fluctuations can be effectively suppressed and no longer dominate the instability of the optical frequencies. In our experiment, we observe that the stability of optical frequency dissemination is improved by more than three orders of magnitude at the integration time of 10,000 s. As a comparison, we measured the floor of optical frequency dissemination by replacing the fiber spool with a 1 m fiber plus a 6-dB attenuator. We can observe that the floor of optical frequency dissemination with a stability of 1.3×10^{-16} at 1 s and 3×10^{-17} at 10,000 s can be obtained. Consequently, the stabilized optical frequency is mainly limited by the noise floor coming from the uncompensated optical paths outside of our interferometer [12], [14], [15].

To examine the mutual effect between two optical frequencies, we disengaged one fiber noise cancellation setup. The fractional instability of each optical frequency is repeatedly measured and the stability for any optical frequency signal remains unchanged, illustrating that the additional optical frequency signal will not sacrifice the performance of optical frequency dissemination. The same phenomenon has also been observed in [30], [34].

C. Radio Frequency Transfer

As the optical frequency transfer is unaffected by the inclusion of RF frequency transmission, we implement RF signal dissemination by engaging both fiber noise cancellation setups. Figure 4 shows the phase noise PSD of the compensated (red trace) and the uncompensated (green trace) RF frequency at 0.9 GHz over the 30 km fiber link. We can clearly see that the phase noise PSD of the free-running RF frequency is significantly higher than the stabilized RF frequency within 100 Hz due to fiber delay fluctuations, mainly induced by the temperature variations and acoustic perturbations. The phase noise PSD of the compensated link in the range of 1 Hz is suppressed by 30 dB, indicating that the lower frequency noise induced by fiber transmission can be suppressed effectively. The compensated RF frequency underperforms the free-running frequency between 100 Hz and 1 kHz, which is mainly due to the unmatched locking bandwidths and gains of the two PID controllers as the strong servo bumps ($\sim$ 1 kHz) shown in the red trace in Fig. 4.

Concerning the RF frequency transfer stability, we measured a fractional frequency stability for the compensated (red filled circles) and the uncompensated (green empty circles) RF frequency with a 5 Hz measurement bandwidth. The results illustrate that we achieve 0.9 GHz RF frequency transfer with a stability of 5.7×10^{-13} at 1 s and 5.2×10^{-16} at 10,000 s, scaling down with $\sim \tau^{-1}$. This is slightly worse than the floor of RF signal dissemination by replacing the fiber spool with a 1 m fiber and a 6 dB optical attenuator as the square markers shown in Fig. 5. Nevertheless, the stability of RF transfer is improved by more than one order of magnitude at the averaging time of 10,000 s.

Here we have to note that this observation is different from the experimental results presented in [30], where the unstabilized RF frequency has no obvious difference with the stabilized case. This is inconsistent with conventional fiber-optic RF dissemination by amplitude modulating a CW laser [8]–[10] in which with and without fiber noise cancellation setups have significantly difference [8]–[10]. The main cause of this situation is probably limited by the uncommon-mode phase noise coming from two different optical paths at the local site and the crosstalk phase noise effect [31].

The RF frequency transfer stability is similar to several other reported techniques (e.g. [35]). Note that the fractional frequency stability of RF frequency dissemination can be improved

Authorized licensed use limited to: Shanghai Jiaotong University. Downloaded on February 06,2021 at 13:16:32 UTC from IEEE Xplore. Restrictions apply.

by increasing the RF frequency. For example, increasing the value of the RF frequency to 9 GHz from 0.9 GHz will not affect the achieved absolute frequency stability, but will improve the fractional frequency stability by one order of magnitude.

IV. Discussion

We have described and experimentally demonstrated the function of a hybrid stabilized RF frequency and optical frequency transfer technique. This technique exploits several advantages of optical phase sensing over other RF frequency transfer techniques, producing a device that is compact in size. By using the AOMs to generate the optical frequency shifts at the local and remote sites, we can avoid the need to use additional lasers at the remote sites to circumvent the effects of unwanted reflections on the transmission link at the local site. Although the Rayleigh backscattering effect can be effectively suppressed at the local site, this still appears at the remote site because the same RF frequency adopted for bidirectional transmissions, resulting in superposing of the back-scattering beatnote on the transferred signal at the remote site [36]. This is one of the main factors limiting the performance of RF transfer results. The effect is clearly illustrated by the lower phase noise PSD in the closed loop than that in the open loop outside the loop bandwidth illustrated in Fig. 4. Note that we measured the open loop phase noise PSD without the backward light, resulting in the Rayleigh backscattering noise-free measurements. By filtering out the two stabilized optical frequencies at the remote site, the stabilized RF frequency without the effect of the backscattering effect can be obtained by beating the two stabilized optical frequencies at a PD. The implement of this technique will be thoughtfully investigated in the immediate next step. Moreover, in comparison with classical RF frequency transfer techniques, a dispersion compensation module is not necessary to prevent phase variations caused by the chromatic dispersion. This way we will fully benefit from the local-remote high stability of the optical carrier and reduce substantially the impact of the fiber chromatic dispersion on RF signal stability [37].

Using equipment readily available in our laboratory we regard the results as not the best case which could be improved by using more specialized components and designs for further improvements. The potential improvement is the spatial design of the fiber-optic setup used for stabilizing of output optical frequencies; the fiber path starting at the input of the EOM at the local site and ending at the remote site is stabilized, but thermal and acoustic perturbations affecting all other fibers or fiber components involved in the optical carrier transfer path. In the current setup, the interferometer was built with an EOM, which caused non-optimal spatial design and thus involved relatively long uncompensated fibers. The long uncompensated fibers will introduce significant phase fluctuations at time scales longer than 1 s because of thermal expansion of the fiber and thermally induced variations in the refractive index [38], [39]. The variations typically depend on the temperature fluctuation cycle. To better understand this factor, here we quantitatively estimate the effect of the temperature variations on the long-term stability. The propagation delay variations $\Delta\tau$ with a fiber link length of Δl due to a sinusoidal time-varying temperature are,

$$\Delta\tau = \frac{\Delta l}{c}(\alpha_n + n\alpha_\Lambda)\Delta T \sin(2\pi t/T_c), \tag{2}$$

where $\alpha_n \approx 1.06 \times 10^{-5}$/K (25 °C room-temperature, 1550 nm) and $\alpha_\Lambda \approx 5.6 \times 10^{-7}$/K (25 °C room-temperature, 1550 nm) are, respectively, the thermo-optic and thermal expansion coefficient of the typical single-mode fiber, n is the effective refractive index of the fiber and ΔT and T_c are the sinusoidal temperature fluctuation peak-to-peak and cycle, respectively. Using Eq. (2), the Allan deviation can be calculated as [40], [41],

$$\sigma_y(\tau) = \frac{2\Delta T \Delta l(\alpha_n + n\alpha_\Lambda)}{c\tau} \sin^2(\pi\tau/T_c). \tag{3}$$

In our typical experimental configuration, the real optical path length, in particular the fiber-pigtailed EOM, is difficult to identify and we estimate the out-of-loop mismatch up to $L = 1$ m. For a typical temperature perturbation with the fluctuation amplitude and cycle of 1 K and 3,600 s, respectively, one expects a bump of the Allan deviation as high as 4×10^{-17} at 1,800 s. Note that the Allan deviation has capability to be improved by two orders of magnitude to 4×10^{-19} at 1,800 s by reducing the unbalanced fiber length to 10 cm and by actively stabilizing the temperature to the level of 0.1 K of the peak-to-peak value with passive or active methods [42]. For field-deployed fibers installed mainly underground and spool fibers in the laboratory, Eq. (3) can also be used for estimating the frequency transfer stability without any phase compensation [38], [39].

To date, efforts have mainly focused on long-distance connections, using methods similar to that proposed in 1994 by Ma *et al.* to correct phase perturbations between the local and remote ends [11]. In recent years, schemes with a variety of different topological structures that are intended to meet multi-access application requirements have been experimentally demonstrated. As proposed by Grosche *et al.* [43], it is efficient to implement a main optical link along which the signal is distributed to multiple users. However, this scheme will face a dilemma that the system will not work properly if the main link servo fails. Another possibility is to implement a branching optical fiber network with phase correction at each output end [44], [45]. A key element of the latter technique is that each remote site requires a unique AOM frequency to distinguish it from the AOM frequencies used by the other remote sites with a frequency multiplexing division technique as illustrated in Fig. 6. Due to the limited bandwidth and the working frequencies of the AOMs, this condition is sometimes difficult to satisfy with the significant increase in the number of users. Fortunately, this will not be an issue by adopting the scheme proposed here because of the large bandwidth of the EOM. However, we have to consider the additional fractional frequency instability coming from the frequency difference between bidirectional optical signals [33]. Although this proposed configuration will increase the complexity of the local site, the maintenance of the whole system is easily achieved at the central office, and the probability of failure at each remote site is massively reduced.

Authorized licensed use limited to: Shanghai Jiaotong University. Downloaded on February 06,2021 at 13:16:32 UTC from IEEE Xplore. Restrictions apply.

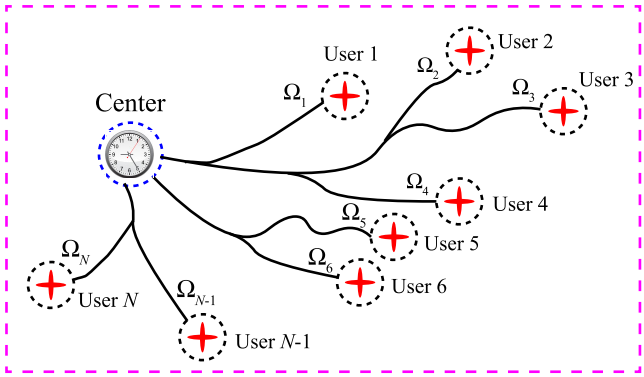

Fig. 6. Diagram of optical frequency dissemination with a star topology. While using the scheme demonstrated here, it will be convenient to simultaneously transfer an optical frequency from a central station to multiple end-users with a frequency division multiplexing technique. The fiber-induced optical phase noise at each user can be compensated by the central station.

V. Conclusion

In this paper, we presented a combined system capable of transferring an RF reference frequency and dual-optical frequencies by adopting a dual-stabilization technique with a single optical actuator. The key innovation of the proposed scheme was finding a way to use a large bandwidth EOM as a frequency shifter for inserting an RF signal between two optical frequencies and as a dual-channel optical actuator for effectively suppressing the phase noise introduced by the fiber. The results demonstrate that we have achieved 193 THz optical carrier dissemination with a stability of 1.2×10^{-15} at the integration time of 1 s and 3.5×10^{-17} at 10,000 s, and 0.9 GHz RF signal dissemination with a stability of 5.7×10^{-13} at 1s and 5.2×10^{-16} at 10,000 s over a 30 km optical fiber link. Delivery of highly stable optical and RF references allows the users to synthesize the signals in bands of optical spectrum as well as in the RF domain. Potential users might be involved in clocks development, high-resolution spectroscopy, radio astronomy observations, relativistic geodesy, tests of fundamental physics and so on.

References

[1] J. Grotti *et al.*, "Geodesy and metrology with a transportable optical clock," *Nat. Phys.*, vol. 14, no. 5, pp. 437–441, 2018.

[2] C. Clivati *et al.*, "A VLBI experiment using a remote atomic clock via a coherent fibre link," *Sci. Rep.*, vol. 7, 2017, Art. no. 40992.

[3] B. Wang, X. Zhu, C. Gao, Y. Bai, J. Dong, and L. Wang, "Square kilometre array telescope—precision reference frequency synchronisation via 1f-2f dissemination," *Sci. Rep.*, vol. 5, 2015, Art. no. 13851.

[4] S. L. Campbell *et al.*, "A fermi-degenerate three-dimensional optical lattice clock," *Science*, vol. 358, no. 6359, pp. 90–94, 2017.

[5] M. Schioppo *et al.*, "Ultrastable optical clock with two cold-atom ensembles," *Nat. Photonics*, vol. 11, no. 1, pp. 48–52, 2017.

[6] C. Lisdat *et al.*, "A clock network for geodesy and fundamental science," *Nat. Commun.*, vol. 7, 2016, Art. no. 12443.

[7] L. Hu, N. Poli, L. Salvi, and G. M. Tino, "Atom interferometry with the Sr optical clock transition," *Phys. Rev. Lett.*, vol. 119, no. 26, 2017, Art. no. 263601.

[8] J. Shen, G. Wu, L. Hu, W. Zou, and J. Chen, "Active phase drift cancellation for optic-fiber frequency transfer using a photonic radio-frequency phase shifter," *Opt. Lett.*, vol. 39, no. 8, pp. 2346–2349, 2014.

[9] R. Huang, G. Wu, H. Li, and J. Chen, "Fiber-optic radio frequency transfer based on passive phase noise compensation with frequency dividing and filtering," *Opt. Lett.*, vol. 41, no. 3, pp. 626–629, 2016.

[10] J. Zhang *et al.*, "Fiber-optic radio frequency transfer based on active phase noise compensation using a carrier suppressed double-sideband signal," *Opt. Lett.*, vol. 42, no. 23, pp. 5042–5045, 2017.

[11] L.-S. Ma, P. Jungner, J. Ye, and J. L. Hall, "Delivering the same optical frequency at two places: Accurate cancellation of phase noise introduced by an optical fiber or other time-varying path," *Opt. Lett.*, vol. 19, no. 21, pp. 1777–1779, 1994.

[12] S. M. Foreman, A. D. Ludlow, M. H. De Miranda, J. E. Stalnaker, S. A. Diddams, and J. Ye, "Coherent optical phase transfer over a 32-km fiber with 1 s instability at 10^{-17}," *Phys. Rev. Lett.*, vol. 99, no. 15, 2007, Art. no. 153601.

[13] P. A. Williams, W. C. Swann, and N. R. Newbury, "High-stability transfer of an optical frequency over long fiber-optic links," *J. Opt. Soc. Am. B*, vol. 25, no. 8, pp. 1284–1293, 2008.

[14] K. Predehl *et al.*, "A 920-kilometer optical fiber link for frequency metrology at the 19th decimal place," *Science*, vol. 336, no. 6080, pp. 441–444, 2012.

[15] S. Droste *et al.*, "Optical-frequency transfer over a single-span 1840 km fiber link," *Phys. Rev. Lett.*, vol. 111, no. 11, 2013, Art. no. 110801.

[16] C. Clivati *et al.*, "Optical frequency transfer over submarine fiber links," *Optica*, vol. 5, no. 8, pp. 893–901, 2018.

[17] D. Calonico *et al.*, "High-accuracy coherent optical frequency transfer over a doubled 642-km fiber link," *Appl. Phys. B*, vol. 117, no. 3, pp. 979–986, 2014.

[18] C. Daussy *et al.*, "Long-distance frequency dissemination with a resolution of 10^{-17}," *Phys. Rev. Lett.*, vol. 94, no. 20, 2005, Art. no. 203904.

[19] G. Marra, H. S. Margolis, and D. J. Richardson, "Dissemination of an optical frequency comb over fiber with 3×10^{-18} fractional accuracy," *Opt. Express*, vol. 20, no. 2, pp. 1775–1782, 2012.

[20] K. Jung, J. Shin, J. Kang, S. Hunziker, C.-K. Min, and J. Kim, "Frequency comb-based microwave transfer over fiber with 7×10^{-19} instability using fiber-loop optical-microwave phase detectors," *Opt. Lett.*, vol. 39, no. 6, pp. 1577–1580, 2014.

[21] S. Nagano *et al.*, "Dissemination of optical-comb-based ultra-broadband frequency reference through a fiber network," *Opt. Express*, vol. 24, no. 17, pp. 19 167–19 178, 2016.

[22] D. J. Jones *et al.*, "Carrier-envelope phase control of femtosecond mode-locked lasers and direct optical frequency synthesis," *Sci.*, vol. 288, no. 5466, pp. 635–639, 2000.

[23] T. Udem, R. Holzwarth, and T. W. Hänsch, "Optical frequency metrology," *Nature*, vol. 416, no. 6877, pp. 233–237, 2002.

[24] C. Grebing *et al.*, "Realization of a timescale with an accurate optical lattice clock," *Optica*, vol. 3, no. 6, pp. 563–569, 2016.

[25] H. Hachisu, F. Nakagawa, Y. Hanado, and T. Ido, "Months-long real-time generation of a time scale based on an optical clock," *Sci. Rep.*, vol. 8, no. 1, 2018, Art. no. 4243.

[26] J. Yao, T. E. Parker, N. Ashby, and J. Levine, "Incorporating an optical clock into a time scale," *IEEE Trans. Ultrason. Ferroelectr. Freq. Control*, vol. 65, no. 1, pp. 127–134, Jan. 2018.

[27] W. McGrew *et al.*, "Towards the optical second: Verifying optical clocks at the SI limit," *Optica*, vol. 6, no. 4, pp. 448–454, 2019.

[28] Z. Feng *et al.*, "High-stability and multithreading phase-coherent receiver for simultaneous transfer of stabilized optical and radio frequencies," *Opt. Lett.*, vol. 44, no. 10, pp. 2418–2421, 2019.

[29] P. Krehlik, H. Schnatz, and Ł. Śliwczyński, "A hybrid solution for simultaneous transfer of ultrastable optical frequency, RF frequency, and utc time-tags over optical fiber," *IEEE Trans. Ultrason. Ferroelectr. Freq. Control*, vol. 64, no. 12, pp. 1884–1890, Dec. 2017.

[30] D. R. Gozzard, S. W. Schediwy, and K. Grainge, "Simultaneous transfer of stabilized optical and microwave frequencies over fiber," *IEEE Photon. Technol. Lett.*, vol. 30, no. 1, pp. 87–90, Jan. 2018.

[31] H. Wei *et al.*, "Frequency crosstalk on fiber-optic radio frequency transfer under fiber temperature variation," *Opt. Eng.*, vol. 58, no. 6, 2019, Art. no. 066117.

[32] V. Ferrero and S. Camatel, "Optical phase locking techniques: An overview and a novel method based on single side sub-carrier modulation," *Opt. Express*, vol. 16, no. 2, pp. 818–828, 2008.

[33] L. Hu, X. Tian, G. Wu, J. Shen, and J. Chen, "Fundamental limitations of Rayleigh backscattering noise on fiber-based multiple-access optical frequency transfer," 2020, *arXiv:2003.13417*.

[34] S. W. Schediwy, D. R. Gozzard, S. Stobie, J. A. Malan, and K. Grainge, "Stabilized microwave-frequency transfer using optical phase sensing and actuation," *Opt. Lett.*, vol. 42, no. 9, pp. 1648–1651, 2017.

[35] D. R. Gozzard, S. W. Schediwy, B. Courtney-Barrer, R. Whitaker, and K. Grainge, "Simple stabilized radio-frequency transfer with optical phase actuation," *IEEE Photon. Technol. Lett.*, vol. 30, no. 3, pp. 258–261, Feb. 2017.

Authorized licensed use limited to: Shanghai Jiaotong University. Downloaded on February 06,2021 at 13:16:32 UTC from IEEE Xplore. Restrictions apply.

[36] T. H. Wood, R. A. Linke, B. L. Kasper, and E. C. Carr, "Observation of coherent Rayleigh noise in single-source bidirectional optical fiber systems," *J. Light. Technol.*, vol. 6, no. 2, pp. 346–352, 1988.
[37] O. Lopez, A. Amy-Klein, M. Lours, C. Chardonnet, and G. Santarelli, "High-resolution microwave frequency dissemination on an 86-km urban optical link," *Appl. Phys. B*, vol. 98, no. 4, pp. 723–727, 2010.
[38] M. Amemiya, M. Imae, Y. Fujii, T. Suzuyama, and S.-i. Ohshima, "Simple time and frequency dissemination method using optical fiber network," *IEEE T. Instrum. Meas.*, vol. 57, no. 5, pp. 878–883, May 2008.
[39] T. Pinkert *et al.*, "Effect of soil temperature on optical frequency transfer through unidirectional dense-wavelength-division-multiplexing fiber-optic links," *Appl. Opt.*, vol. 54, no. 4, pp. 728–738, 2015.
[40] J. A. Barnes *et al.*, "Characterization of frequency stability," *IEEE T. Instrum. Meas.*, vol. IM-20, no. 2, pp. 105–120, May 1971.
[41] S. T. Dawkins, J. J. McFerran, and A. N. Luiten, "Considerations on the measurement of the stability of oscillators with frequency counters," *IEEE Trans. Ultrason. Ferroelectr. Freq. Control*, vol. 54, no. 5, pp. 918–925, May 2007.
[42] S. Droste, "Optical frequency transfer via telecommunication fiber links for metrological applications," Ph.D. dissertation, Gottfried Wilhelm Leibniz Universität Hannover, Hannover, Germany, 2014.
[43] G. Grosche, "Eavesdropping time and frequency: Phase noise cancellation along a time-varying path, such as an optical fiber," *Opt. Lett.*, vol. 39, no. 9, pp. 2545–2548, 2014.
[44] S. W. Schediwy *et al.*, "High-precision optical-frequency dissemination on branching optical-fiber networks," *Opt. Lett.*, vol. 38, no. 15, pp. 2893–2896, 2013.
[45] L. Wu, Y. Jiang, C. Ma, H. Yu, Z. Bi, and L. Ma, "Coherence transfer of subhertz-linewidth laser light via an optical fiber noise compensated by remote users," *Opt. Lett.*, vol. 41, no. 18, pp. 4368–4371, 2016.

Xueyang Tian received the B.S. degree from Shanghai Dianji University, China, in 2017. She is currently a graduate student in the State Key Laboratory of Advanced Optical Communication Systems and Networks, Department of Electronic Engineering, Shanghai Jiao Tong University, China. Her current research interests include photonic signal transmission.

Liang Hu (Member, IEEE) received the B.S. degree from Hangzhou Dianzi University, China, in 2011, and the M.S. degree from Shanghai Jiao Tong University, China, in 2014. He received the Ph.D. degree from University of Florence, Italy, in 2017 during which he was a Marie-Curie Early Stage Researcher at FACT project. He is currently a Tenure-Track Assistant Researcher in the State Key Laboratory of Advanced Optical Communication Systems and Networks, Department of Electronic Engineering, Shanghai Jiao Tong University, China. His current research interests include photonic signal transmission and atom interferometry.

Guiling Wu (Member, IEEE) received the B.S. degree from Haer Bing Institute of Technology, China, in 1995, and the M.S. and Ph.D. degrees from Huazhong University of Science and Technology, China, in 1998 and 2001, respectively. He is currently a Professor in the State Key Laboratory of Advanced Optical Communication Systems and Networks, Department of Electronic Engineering, Shanghai Jiao Tong University, China. His current research interests include photonic signal processing and transmission.

Jianping Chen received the B.S. degree from Zhejiang University, China, in 1983, and the M.S. and Ph.D. degrees from Shanghai Jiao Tong University, China, in 1986 and 1992, respectively. He is currently a Professor in the State Key Laboratory of Advanced Optical Communication Systems and Networks, Department of Electronic Engineering, Shanghai Jiao Tong University. His main research interests include opto-electronic devices and integration, photonic signal processing, and system applications. He is a Principal Scientist of National Basic Research Program of China (also known as 973 Program).

Authorized licensed use limited to: Shanghai Jiaotong University. Downloaded on February 06,2021 at 13:16:32 UTC from IEEE Xplore. Restrictions apply.